Size-Controlled Synthesis of Nano-Zeolites and their Application to Light Olefin Synthesis

Teruoki Tago, Hiroki Konno, Yuta Nakasaka, Takao Masuda

Division of Chemical Process Engineering, Faculty of Engineering, Hokkaido University

N13W8, Kita-Ku Sapporo, Hokkaido, 060-8628, Japan

Corresponding author: T. Tago, tago@eng.hokudai.ac.jp

Abstract

For the application of zeolites as heterogeneous catalysts, low diffusion resistance for hydrocarbons within the micropore is essential for improving product selectivity and catalyst lifetime. This problem has been overcome by reducing the crystal size. This review introduces size-controlled preparation of nano-sized zeolites *via* hydrothermal synthesis in water/surfactant/organic solvent (emulsion method) and their application to heterogeneous catalysts. The ionicity of the hydrophilic group in surfactant molecules and the concentration of the Si source affected the crystallinity and morphology of zeolites prepared using the emulsion method. When using a non-ionic surfactant, mono-dispersed silicalite-1 nanocrystals approximately 60 nm in diameter were successfully prepared. Nano- and macro-ZSM-5 zeolites with crystal sizes of approximately 150-200 nm and 1.5 μm, respectively, were prepared and applied to *n*-hexane cracking and acetone-to-olefin reactions to investigate the effect of zeolite crystal size on catalytic stability and light olefin yield. Application of nano-zeolite to light olefin production was effective in achieving faster mass transfer of hydrocarbon molecules within the micropore, which led to improvements in olefin yields and catalyst lifetime.

Keywords

Nano-zeolite, Surfactant, Light olefin, *n*-Hexane cracking, Acetone to olefin

1 Introduction

Zeolites, defined as crystalline and porous aluminosilicates (or other metal oxides), possess three-dimensionally connected framework structures constructed from corner-sharing TO_4 tetrahedra, where T is any tetrahedrally-coordinated cation such as Si or Al. These framework structures are composed of *n*-rings, where *n* is the number of T-atoms in the ring (*e.g.*, 4-, 5-, or 6-membered rings), and large pore openings of 8-, 10-, and 12-membered rings are framed by these small rings. Figure 1 shows the pore sizes and framework structures of typical zeolites. The sizes of the intracrystalline pores and nanospaces, which depend on the type of zeolite providing the framework, are close to the molecular diameters of lighter hydrocarbons. In addition, strong acid sites exist on the nanopore surfaces within the zeolite crystal and on the external surface of the crystal. These properties enable the use of zeolites in reaction processes (shape-selective catalysts such as fluid catalytic cracking of heavy oil, isomerization of xylene, and synthesis of ethyl-benzene) and separation processes (adsorptive- and membrane-separation).

However, the crystal sizes of zeolites are very large (approximately 1–3 μm) compared to the size of micropores possessing a molecular-sieving effect. When the zeolite is used as a shape-selective catalyst, the reaction apparently is limited by diffusion of reactant molecules within the zeolite crystals, leading to low product selectivity. In addition, since effective active sites (acid sites) for catalytic reactions are distributed on internal surfaces of the main channels and on external surfaces of the crystal, the pore mouths are plugged easily due to coke deposition,

leading to short catalyst lifetimes. Faster mass transfer is required to avoid these serious problems, which resulted in two primary strategies to provide faster mass transfer: formation of meso-pores within zeolite crystals [1-3], and preparation of nano-zeolites [4-16]. In nano- zeolites, the diffusion length for reactant hydrocarbons, assignable to crystal size, decreases, and the external surface area of the crystal increases as crystal size decreases. The increase in external surface area and the decrease in diffusion resistance are effective for improving catalytic activity in gas-solid and liquid-solid heterogeneous catalytic reactions. Because of the favorable properties of nano-zeolites for catalytic reactions, preparation methods for several types of nano-zeolites have been reported and reviewed [17, 18].

This review describes a method for preparing nano-zeolites in a solution consisting of a surfactant, organic solvent, and water (called the emulsion method [19-23]). The nano-zeolite is a promising material for increasing external surface area as well as decreasing diffusion resistance of the organic reactant within the micropores, thereby improving catalytic activity and lifetime. In addition, deactivation of acid sites of the zeolite using an organic silane compound improves the zeolitic properties when applying nano-zeolites to heterogeneous catalytic reactions. A new method based on catalytic cracking of silane (called the CCS method [24-26]) is also described. Finally, light olefin synthesis *via* *n*-hexane cracking and acetone-to-olefin reaction over nano-zeolites, which successfully produce high yields of the light olefin with long catalyst life, is outlined.

2 Syntheses of Nano-Zeolites

2.1 Synthesis of Nano-Zeolites in Water/Surfactant/Organic Solvent

Typical preparation of zeolites involves an aqueous solution containing Si and Al sources and alkaline metal ions (sodium or potassium). An organic structure directing agent (OSDA), such as an ammonium alkyl cation, is also necessary to form the zeolite framework during synthesis of some types of zeolite [*e.g.*, tetra-*n*-methyl ammonium hydroxide (TMA-OH) for FAU zeolite; tetra-*n*-ethyl ammonium hydroxide (TEA-OH) for BEA and MOR zeolites; and tetra-*n*-propyl ammonium hydroxide (TPA-OH) for MFI zeolite]. For one conventional method of zeolite preparation, an aqueous solution containing the inorganic compounds and OSDA is simply poured into a Teflon-sealed stainless bottle, heated to the required temperature and subjected to hydrothermal synthesis. Zeolite crystals with different properties (acidity and framework topology) can be prepared by changing the type of OSDA and varying the concentrations of Si, Al, and OSDA, including the molar ratios of Si/Al and Si/OSDA in the aqueous solution.

For this conventional method, crystal nucleation occurs first, followed by growth of the zeolite, with nucleation simultaneously occurring during the growth stage. As concentrations of the Si and Al sources increase, the nucleation rate also increases, leading to a decrease in zeolite crystal size. However, zeolites obtained by this method often have a broad size distribution due to simultaneous nucleation and crystal growth during hydrothermal treatment. Accordingly,

separation of the nucleation and growth stages is very important for obtaining the nano-zeolites. Interest has been growing in synthesis of nano-zeolites from addition of surfactants, including those prepared in a water/surfactant/organic mixture [19-23, 27-29] (emulsion method), where the focus is on size and morphology control.

For the emulsion method, two solutions are prepared: an aqueous solution containing the Si and Al sources and OSDA molecules, and an organic solvent containing the surfactant molecules. The aqueous solution is added to the surfactant/organic solution, and the mixture is stirred to obtain a homogeneous solution. Then, the resulting mixture of water/surfactant/organic solvent is placed in a Teflon-sealed stainless steel bottle, heated to 373 to 453 K, and held at the required temperature for 12 to 120 h with stirring to yield nano-sized zeolites. Unlike the conventional method, three additional parameters, ionicity of surfactant [19, 20], water-to-surfactant molar ratio [21], and concentration of surfactant in the organic solvent [22, 23] are important in the emulsion method, because these parameters affect crystallinity, morphology and crystal size. Thus, the effects of these parameters are described in detail, using the preparation of silicalite-1 (MFI zeolite) as an example.

2.2 Effects of Surfactant Ionicity on Preparation of Nano-Zeolites

Surfactant molecules possess both hydrophobic (lipophilic) and hydrophilic groups. Because the hydrophilic groups have an electric charge, the surfactant molecule can adsorb onto a solid

surface due to the electrostatic interaction, thus reducing the interface energy difference between the solid surface and solvent, and enhancing nucleation of the metal and/or metal oxide nano-particles. The interaction between the surfactant and the surfaces of the zeolite nuclei and crystals is an important factor affecting crystallinity and crystal size; therefore, the effect of ionicity of surfactant on crystallinity of silicalite-1 has been investigated.

In general, four types of surfactants exist: anionic, cationic, non-ionic, and bipolar. The present review examined nonionic surfactants [*e.g.*, polyoxyethylene(15)oleylether (O-15), polyoxyethylene(15)nonylphenylether (N-15), and poly(oxyethylene)(15)cetylether (C-15)] and ionic surfactants [*e.g.*, sodium bis(2-ethylhexyl) sulfosuccinate (AOT) and cetyltrimethyl ammonium bromide (CTA-Br)]. Cyclohexane or 1-hexanol was used as the organic solvent. Silicalite-1 crystals were prepared using the emulsion method at a hydrothermal temperature of 140 °C and a surfactant concentration of 0.50 mol/L in the organic solvent. Tetraethyl orthosilicate and tetra-*n*-propyl ammonium hydroxide (TPA-OH) were used as a Si source and OSDA, respectively. Figure 2 shows FE-SEM images of the samples obtained. The FE-SEM image of the sample prepared by the conventional hydrothermal method is also shown for comparison.

The sample prepared in the AOT/cyclohexane solution [Fig. 2(a)] showed irregular morphology without crystalline silicalite-1. In this situation, TPA-OH molecules did not act as an OSDA in the synthetic solution, possibly because the AOT and TPA-OH used as the OSDA have opposite ionic charges. For the sample prepared in CTA-Br/1-hexanol [Fig. 2(b)], coexistence of

silicalite-1 crystals and amorphous SiO_2 was observed. Because the molecular structure of CTA-Br is similar to that of TPA-OH, these molecules can adsorb onto the silica surface during hydrothermal synthesis, leading to separate formation of amorphous SiO_2 and silicalite-1 crystals due to independent adsorption of CTA^+ and TPA^+, respectively. In contrast, for samples prepared in cyclohexane with nonionic surfactants (O-15, C-15, and N-15), mono-dispersed silicalite-1 nanocrystals were obtained [Figs. 2(c)]. SEM pictures of the sample prepared in water (without surfactant) showed a heterogeneous structure of smaller crystals (diameter of approximately 30 nm) on larger crystals (approximately 120 nm) [Fig. 2(d)], indicating that nucleation, crystallization, and crystal growth occurred simultaneously. In the emulsion method, aggregation of silicalite-1 nuclei is inhibited by surfactants adsorbed on the surface during hydrothermal treatment, which allows the preparation of mono-dispersed nano-zeolites. These results indicate that the ionicity of hydrophilic groups in the surfactant molecules is important in the formation and crystallization processes of nano-zeolites [19].

2.3 Effects of Surfactant Concentration and Water-to-Surfactant Molar Ratio (W/S value) on Silicalite-1 Crystal Size

The effects of the the synthetic solution composition, such as surfactant concentration and amount of water, on the morphology and crystal size of silicalite-1 nanocrystals were examined. Concentration of the Si source in the water was 1.6 mol/L, and the molar ratio of Si to OSDA

(TPA-OH) was Si/TPA-OH=3. Surfactant concentration and amount of aqueous solution ranged from 0.1–0.75 mol/L, and from 2.5–15 mL, respectively.

The relation between size of the silicalite-1 crystals and composition of the synthetic solution (surfactant concentration and amount of aqueous solution) is summarized in Fig. 3. The FE-SEM photographs of typical samples are also shown. The vertical and horizontal axes indicate the volume of aqueous solution added and the surfactant concentration in the organic solvent (70 ml), respectively. Percentages below the symbols showed yields of silicalite-1. The W/S values in the figure are the molar ratio of water to surfactant. The straight lines in the figure represent the lines with constant W/S values. Prior to hydrothermal synthesis, the water-surfactant-organic solvent was homogeneous and clear at W/S values less than 22, and heterogeneous at a W/S value of 54.

X-ray diffraction confirmed that these samples were MFI zeolite crystals. Crystal morphology and size varied widely among the samples, while the composition of the aqueous solution and hydrothermal conditions remained uniform. The W/S value also affected crystal size. As W/S values decreased from 54, crystal size of silicalite-1 decreased, reaching a minimum 60 nm at a W/S value of 11. Crystal size then increased as the W/S values continued to decrease. These results indicate that crystal size depended on surfactant concentration and the amount of aqueous solution added to the surfactant-organic solvent, which may affect the rates of nucleation and crystal growth of silicalite-1, causing a change in crystal size with changes in W/S values [21].

In the emulsion method, the adsorbing surfactants on the surface of the silicalite-1 precursor contributed to suppression of dissolution of the precursor into the solution, enhancing the nucleation rate [22, 23]. In addition, since the nucleation of silicalite-1 was completed during the initial stage of hydrothermal synthesis, subsequent crystal growth led to the successful preparation of mono-dispersed silicalite-1 nanocrystals. Accordingly, at W/S 11, the silicalite-1 nanocrystals were small (approximately 60 nm), with a narrow size distribution. Moreover, as the surfactant concentration increased up to 0.75 mol/L (W/S=3), stabilization of the precursor was enhanced due to an increase in the amount of adsorbed surfactants, which restricted collisions of the precursor to form zeolite nuclei as compared with W/S 11. This stabilization produced a preference for crystal growth after nucleation, leading to increasing crystal size up to approximately 1000 nm.

2.4 Mechanism

To determine the mechanism of zeolite nanocrystal formation in a water/surfactant/organic mixture, the relation between ionicity of the surfactant and the OSDA molecule, and the ionic charges of the SiO_2 surface and/or zeolite precursor were investigated in detail. In the method, the cyclohexane used as the organic solvent contributes to stabilization of the hydrophobic group of the surfactant. Effect of ionicity of the hydrophilic group of the surfactant and the composition of the water/surfactant/organic solvent on morphology and crystallinity of the silicalite-1

nanocrystals obtained are shown in Figs. 2 and 3. A schematic diagram showing zeolite nucleation, crystal growth, and a possible relation between the surfactant and zeolite surface is shown in Fig. 4.

Davis *et al*. [30-33] reported a synthetic mechanism of silicalite-1 formation for which nucleation and crystal growth were composed of two steps: 1) formation of aggregates (5–10 nm) by collisions of zeolite precursors (2.8 nm) consisting of poly-silicate ions and OSDA molecules, and 2) transformation of the aggregates into silicalite-1 nuclei followed by crystal growth of the nuclei by collisions of precursors. As shown in Fig. 2, the silicalite-1 crystal prepared by the conventional method (in water solution without surfactant) had a broad size distribution, resulting from simultaneous nucleation and crystal growth due to the high Si concentration (1.6 mol/L).

A hydrophilic group of surfactant O-15 is composed of poly-oxyethylene chains, making it a non-ionic surfactant. In contrast, the surface of the zeolite precursor and crystal are composed of a hydrophobic surface (-Si-O-Si-) and hydrophilic silanol groups (-O-Si-OH). The hydrophilic groups of the surfactant can be adsorbed on the hydrophilic silanol groups, leading to stabilization of the silanol groups. On the hydrophobic surface, hydrophobic hydration occurs in the conventional preparation method without a surfactant [30-33]. The hydrophilic groups of the surfactant are likely adsorbed onto the water molecules hydrophobically hydrated on the zeolite surface. Moreover, the hydrophobic (lipophilic) group of the surfactant can be adsorbed on the hydrophobic surface. These adsorbed surfactants can contribute to stabilization of the surface of zeolite precursor and crystals, which influences the nucleation rate of zeolites [21-23]. The

aggregation and nucleation of the precursors are considered to be complete during the initial stage of hydrothermal synthesis, and subsequent crystal growth leads to the successful preparation of mono-dispersed zeolite nanocrystals.

As shown in Fig. 4, the adsorbing surfactant on the surface of zeolite precursor and nuclei influenced the nucleation and growth rate of zeolites as well as their crystallinity. Because the surface of the zeolite precursor and crystal are composed of hydrophobic and hydrophilic parts, the balance between hydrophilic and lipophilic properties of the surfactat affects the adsorption ability of surfactants on the zeolite surface. Therefore, to investigate the effect of the hydrophilic/lipophilic balance on crystal growth of zeolite in detail, OSDA-free synthesis for ZSM-5 zeolite (MFI zeolite) was conducted, during which non-ionic surfactants without organic solvent were added in the synthetic solution. Non-ionic surfactants containing different polyoxyethylene chain length, such as polyoxyethylene(*n*)oleylether (O-*n*) and poly(oxyethylene)(*n*)cethylether (C-*n*), were added to the synthetic solution. The Si concentration and Si/Al ratio were 1.0 mol/L and 50, respectively, and the ratio of oxyethylene groups to Si moles [(CH_2CH_2O)/Si] was kept at a constant value of 1.6. The hydrophilic and lipophilic balance (HLB) value of the surfactants was calculated using the Kawakami method [34, 35]:

$$\text{HLB value} = 7 + 11.7\log(M_W/M_O) \quad (1)$$

where M_W and M_O represent molecular weights of the hydrophilic and lipophilic groups of the surfactant, respectively. As the chain length of the hydrophilic group increases, the hydrophilic property of the surfactant increases along with the HLB value.

XRD patterns of samples obtained showed peaks corresponding to MFI zeolites in OSDA-free conditions, regardless of surfactant addition and types of surfactat added, so the difference in crystallinity of the obtained samples from the XRD patterns were difficult to determine. Accordingly, N_2 adsorbed within a micropore (P/P_0 around 0.0) was used for evaluating the crystallinity of the ZSM-5 obtained. Figure 5 shows the relation between amount of adsorbed N_2 and HLB values of the surfactant. In well-crystallized MFI zeolite prepared using OSDA (TPA-OH), the amount of adsorbed N_2 usually reaches approximately 90 mL/g. The ZSM-5 zeolite prepared in OSDA-free conditions and without surfactant showed insufficient adsorption amount of N_2, about 50 mL/g due to low crystallinity, whereas ZSM-5 prepared with surfactant showed improved crystallinity. Since the pH of the solution was highly alkaline at high temperautres during hydrothermal synthesis, zeolite crystallization, resolution of silica species, and re-precipitation proceeded simulteneously, leading to low zeolite crystallinity due to formation of amorphous silica. Upon surfactant addition, the amount of adsorbed N_2 increased as theHLB value, and exhibited a maximun value near an HLB value of 10-12, corresponding to O-15, where the amount of adsorbed N_2 reached nearly the same value as that for the MFI zeolite prepared using OSDA. This resulted from affinity of the surfactant to the zeolite surface. Because the surfaces of the zeolite precursor and crystal are composed of hydrophobic surface (-Si-O-Si-) and hydrophilic silanol (-O-Si-OH) groups, an optimun HLB value was expected to exist. Because the surfactant molecules could stabilize the surfaces of zeolite nuclei and crystal against resolution of Si species to synthetic solutoin, this improved the crystallinity of ZSM-5 under OSDA-free

conditions. In addition, the stabilization effect of the surfactant on the surfaces of zeolite presursors and nuclei enhanced the nucleation rate of zeolite in the emulsion method, as shown in Fig. 4, leading to the successful preparation of nano-zeolites.

3 Regioselective Deactivation of Acid Sites

3.1 Catalytic Cracking of Silane Method

Because zeolites contain micropores of a specific diameter almost equal to the molecular sizes of lighter hydrocarbons, they can act as a molecular sieve for these hydrocarbons. In lighter olefin synthesis using zeolite catalysts, the spatial limitations within the zeolitic pores should provide effective reaction fields. Unfortunately, reactions over acid sites located on the external surface of the zeolite crystals can give rise to aromatics formation. Moreover, strong acidity with a low Si/Al ratio can cause excessive reaction of the lighter olefins to produce aromatics and coke, leading to short catalyst lifetime. Therefore a strong demand exists for methods that allow deactivation and/or modification of zeolite acidity.

Ion-exchange methods using alkaline and/or alkaline-earth metal ions can decrease and/or deactivate the acidic properties of zeolites, and the other method is silica (SiO_2) formation on the zeolite surface. Niwa *et al.* [36–38] developed a method utilizing chemical vapor deposition (CVD) with tetraethoxysilane and/or tetramethoxysilane precursors to form a thin SiO_2 layer on

the external surface of zeolite crystals. Another proposed method for SiO_2 formation is based on catalytic cracking of silane (CCS method) using organic silane compounds, in which SiO_2 formation selectively occurs on the acid sites of the zeolite [24-26].

For the CCS method, deactivation and/or modification of the acid sites of the zeolite can be achieved by SiO_2 unit formation, which occurs *via* a silane compound chemisorbed on the acid site of the zeolite. The procedure for the CCS method is outlined in Fig. 6 [24, 26]. After air calcination, the zeolite is exposed to vapor of the silane compound at 373 to 393K in a N_2 stream, and then the feed of the silane compound is stopped to remove the silane compounds physically adsorbed on the zeolite surface. Here, the silane compounds chemically adsorbed are remained on the acid sites of the zeolite. Next, the sample is heated to 823K in a N_2 stream to decompose the organic groups of silane compounds adsorbed on acid sites, resulting in formation of silicon-coke composites on the acid sites. Finally, the gas feed flowing around the zeolite is switched from N_2 to air, and the temperature of the reactor is held at 823K in an air stream for 60 min, causing the silicon–coke compounds formed on the acid sites to SiO_2 units. Thus, formation of SiO_2 units occurs on the acid sites that initially chemisorbed the silane compounds. By repeating the sequence two or three times, the formation of SiO_2 units occurs again on the acid sites, leading to a decrease in zeolite acidity.

The changes in acidity of beta zeolite (BEA zeolite) after ion-exchange and CCS treatments are shown in Figs. 7(a) and 7(b), where the effects of these treatments on acidity were clearly demonstrated by NH_3-TPD profiles. An alkaline metal cation and phenyl-silane were used as the

ion-exchanged metal and organic-silane compound, respectively. The peak in the high-temperature region is associated with desorption of NH_3 adsorbed on the strong acid sites, whereas the peak in the low-temperature region is assigned to NH_3 weakly held by or physically adsorbed on the zeolite. The H-beta zeolite exhibited two NH_3 desorption peaks, corresponding to strong and weak acid sites. After ion-exchange, the desorption peak in the high-temperature region (above 600K) indicative of strong acid sites effectively decreased and/or disappeared when compared to the H-beta zeolite [39]. In contrast, after CCS treatment, the amount of NH_3 desorbed form the acid sites decreased in accordance with the number of treatments, but small amounts of strong acid sites still existed after the treatment, because the silanol group on the SiO_2 unit formed on the acid sites by CCS treatment behaves as a new acid site with weaker strength than that before the treatment.

The pore size of the zeolite is expected to decrease slightly after CCS treatment [24]. The diameter of a silicon cation with a coordination number of 4 is about 0.08 nm, hence, the pore size at locations where SiO_2 units have formed should decrease with the size of SiO_2. Consequently, the SiO_2 formed by the CCS method can reduce the acidity and pore size of the zeolite, leading to suppression of formation of aromatics from olefins due to improved spatial limitation.

3.2 Regioselective Deactivation of Acid Sites by CCS Method

In the CCS method, several types of silane compounds can deactivate the acid sites of zeolite, including those with methyl, ethoxy, and phenyl substituents [diethoxymethylsilane (DEM-silane), phenylsilane (P-silane), diphenylsilane (DP-silane), diphenylmethylsilane (DPM-silane), and triphenylsilane (TP-silane)]. Because the molecular size of the silane compound depends on the organic groups bonded to the Si atom, the order of molecular sizes of the silane compounds is as follows (with the pore size of the MFI and BEA zeolites included for comparison); TP-silane > pore diameter of BEA (12-membered rings) > DPM-silane ≈ DP-silane ≈ pore diameter of MFI (10-membered rings) > P-silane > DEM-silane. Therefore, selective deactivation of the acid sites located on the external surface of the zeolite crystals can be achieved by utilizing the molecular sieving effect of the zeolites for silane compounds depending on size. Figure 6 shows a schematic diagram of the selective deactivation of acid sites in the CCS method, according to the relation between molecular diameter of the silane compound and the pore size of zeolite.

The changes in acidity of ZSM-5 zeolite (MFI zeolite) after CCS treatment using different types of silane compounds are shown by the NH_3-TPD profiles in Fig. 8, which clearly indicates the effects of molecular size of the silane compound on acidity. For organic silane compounds having a molecular size similar to the pore size of the ZSM-5 (*e.g.*, DP- and DPM-silanes) or are larger (e.g. TP-silane), selective deactivation occurs at acid sites located near the external surface of the ZSM-5 crystal. In this case, because the decrease in the number of acid sites corresponds to those deactivated acid sites located near the external surface, unmodified acid sites remain inside the crystal. Accordingly, the changes in acidity, such as number of acid sites and acid strength, are

small. The regioselective deactivation of acid sites located near the external surface of ZSM-5 zeolite crystal effectively suppressed undesirable reactions such as aromatics formation and coke deposition in the acetone-to-olefins (ATO) reaction [25, 26]. Moreover, regioselective deactivation in the CCS method using TP-silane could be applied to the ZSM-5 zeolite membrane, where the acid sites located on the external surface of the membrane were selectively deactivated without deactivation of acid sites in the zeolite pores. In methanol-to-olefins (MTO) reaction using the membrane [40], undesirable reactions of methanol to aromatics and coke were suppressed on the membrane surface facing the feed side of methanol, which increase olefin yields [41].

In contrast, when silane compounds smaller than the zeolite pores were used (*e.g.*, DEM- and P-silanes), SiO_2 formation can occur on pore surfaces within the crystal as well as near the external surface. In this case, because the acid sites are accessible for these silane compounds, almost all of the acid sites can be deactivated, decreasing the pore size of ZSM-5 zeolites. A ZSM-5 zeolite membrane after CCS treatment using these silane compounds exhibited improved properties for separation of H_2 from an H_2/N_2 mixture due to pore sizes that were smaller than those before CCS treatment [24].

As a result, different acid site distributions on the zeolite can be accomplished by regioselective deactivation using silane compounds with different molecular sizes, and the method can improve the catalytic and membrane properties.

4 Application of nano-zeolite

4.1 Catalytic Reaction

Alkylation, isomerization and dehydration occur on the acid sites of zeolites which are distributed on the nanopore surfaces and external surfaces of the zeolite crystal. Moreover, because the sizes of the intracrystalline nanospaces are similar to molecular sizes of lighter hydrocarbons, the zeolite can act as a molecular sieve for lighter hydrocarbons.

Hydrocarbon molecules with sizes larger than the pore opening cannot diffuse into zeolite pores, and are adsorbed mainly on the external surface where the catalytic reaction proceeds. As the crystal size of zeolites decreases, the external surface area of the zeolite increases (*e.g.*, in MFI zeolites, about 80 and 10 m^2/g for nano- and macro-zeolites, respectively, as calculated by the t-method) [26]. Consequently, the nano-sized zeolite is effective in increasing catalytic activity for hydrocarbons with large molecular size. Song *et al.* [10, 11] reported the effects of crystal size on adsorption properties of toluene on the zeolite, in which zeolites with crystal sizes less than 100 nm have a higher adsorption capacity for toluene. Botella *et al.* [42] reported the Beckmann rearrangement reaction over nano-beta zeolite, where the reactions proceed mainly on the external surface of the zeolite. Serrano *et al.* [43] reported catalytic cracking of polyolefins over nano-ZSM-5 zeolite. Because the molecular size of polyolefins is larger than the pore size, cracking of polyolefins occurs mainly over the acid sites on the external surface, followed by the

formation of lighter olefins on the internal pore surface. Recently, hierarchical-structured zeolites have attracted attention because nano-pores (called as nanomorphic zeolite) [44, 45] and meso-pores [46-52] are formed among nano-zeolite crystals. The hierarchical materials composed of nano-sized zeolites possess two main advantages: a large external surface area ascribable to nano-zeolite, and larger pores than the zeolitic pore allowing large molecules to reach active sites. For these reasons, the hierarchical zeolites composed of nano-sized ZSM-5 [53] and TS-1 [54] exhibited high activity for polyolefin cracking and olefin epoxidation, respectively.

In contrast, as compared with the pore sizes of zeolite, the molecular sizes of lighter olefins, such as ethylene, propylene and butylene, are enough small to diffuse into the pore, so that the spatial limitations within the zeolite channels provide effective reaction fields for increasing olefin yields. Promising candidate routes for producing light olefins include catalytic cracking of naphtha [55-58] and oxygen-containing chemicals to olefins, such as methanol-to-olefins (MTO) [59, 60], ethanol-to-olefins (ETO) [61-64], and acetone-to-olefins (ATO) [65-71]. In these olefin syntheses, the initial products consist mainly of lighter olefins such as ethylene, propylene and butylene. However, the lighter olefins tend to convert to aromatics and coke due to excessive reaction, hence, low diffusion resistance is required to suppress excessive reaction. Because the diffusion length for the reactant/product hydrocarbons, assignable to crystal size, decreases with crystal size, the nano-zeolite is expected to be an appropriate catalyst to produce light olefins.

4.2 Catalyst for Light Olefin Synthesis

The effect of the crystal sizes of ZSM-5 zeolite (MFI zeolite) affected olefin yields and catalyst lifetime during n-hexane cracking and acetone-to-olefins reaction (ATO reaction). A nano-ZSM-5 zeolite was prepared *via* hydrothermal synthesis using a water/surfactant/organic solvent (emulsion method). An aqueous solution containing the Si and Al source material was obtained by hydrolyzing each metal alkoxide in a dilute tetra-propyl-ammonium hydroxide (TPA-OH)/water solution. Poly-oxyethylene-(15)-oleylether and cyclohexane were used as the surfactant and organic solvent, respectively. To obtain macro-zeolite, hydrothermal synthesis was also conducted without the surfactant/organic solvent (conventional method). Figures 9 and 10 show FE-SEM photographs and NH_3-TPD profiles, respectively, of nano- and macro-zeolites prepared for olefins synthesis. ZSM-5 zeolites with crystal sizes of approximately 150 nm and 1500 nm (nano- and macro-zeolites, respectively) could be obtained. The Si/Al ratio of these zeolites was evaluated by XRF (X-ray Fluorescence meter; Supermini Rigaku Co. Ltd.), and the NH_3-TPD profiles and the Si/Al ratio demonstrated that these zeolites similar Si/Al ratios and acidity regardless of crystal size. The BET and external surface areas of these zeolites were calculated by BET and t-methods, respectively, using N_2 adsorption-desorption isotherms. While the BET surface areas of these zeolites exhibited values similar to 400 m^2/g, the external surface areas were very different. The external surface area of the nano-zeolite was 50 m^2/g, which is much larger than that of the macro-zeolite (10 m^2/g).

4.3 *n*-Hexane Cracking over Nano-Sized Zeolite

Light olefins have been produced mainly by thermal cracking of naphtha, which provides yields of ethylene and propylene of approximately 25% and 13%, respectively. However, because the naphtha cracking process consumes more than 30% of the total amount of energy required in petrochemical refinement, developing efficient processes for production of light olefins is important. In contrast, the catalytic cracking of naphtha over solid-acid catalysts can be achieved at a high propylene/ethylene ratio at low reaction temperatures as compared with thermal cracking [55], so that use of this process could provide energy savings along with the selective production of propylene. Promising catalysts for naphtha cracking including zeolites, and research into catalytic cracking of alkane over various zeolites such as FAU, BEA, MOR, MWW, and MFI have been reported [55-58, 72-79].

Cracking of *n*-hexane over zeolite catalysts, as a model reaction for the catalytic cracking of naphtha, was conducted using a fixed-bed reactor at a reaction temperature of 823K under N_2 at atmospheric pressure. The nano- and macro-sized ZSM-5 zeolites (Si/Al=150) with crystal sizes of approximately 150 nm and 1500 nm (see Fig. 9) were employed as catalysts. The *W/F* value (*W*: amount of catalyst /g, *F*: feed rate /g h^{-1}) was 0.5 h. The feed rate of *n*-hexane (*F*) and catalyst weight (*W*) were 1.37×10^{-2} mol/h and 0.589 g, respectively. The composition of the exit gas was measured by on-line gas chromatography (GC-2014, Shimadzu Co. Ltd.) using a Porapak-Q column for TCD detector, and Gaskuropack and SP-1700 columns for FID detectors. The amount

of coke deposited on the catalyst after reaction was measured by thermogravimetry (TG; TGA-50, Shimadzu Co. Ltd.).

First, the reaction mechanism for *n*-hexane cracking was investigated at a reaction temperature of 823K using ZSM-5 with different Si/Al ratios (50, 80, 150, and 300). Figure 11 shows the effect of Si/Al ratio on catalytic activity and product yields of *n*-hexane cracking. Products including alkanes (methane, ethane, propane, and butane), alkenes (ethylene, propylene, and butylene) and aromatics [benzene, toluene, and xylene (BTX)] were obtained. At low *n*-hexane conversion (Si/Al = 300), propylene and butylene were the major products, because they are formed *via* energetically favorable secondary or tertiary carbenium ions in the classical bimolecular mechanism [80-82]. In contrast, because ethylene is formed *via* energetically unfavorable primary carbenium ions (regardless of the monomolecular or bimolecular mechanism), the yield of ethylene was low. As the conversion increased (*i.e.*, decreasing Si/Al ratio), the yield of BTX increased whereas the yields of propylene and butylene were almost unchanged, indicating that the products from cracking changed in accordance with a series of reactions. Moreover, the yields of methane and ethane increased with *n*-hexane conversion. Methane and ethane are formed *via* a monomolecular mechanism, as described by Haag and Dessau [83]. As a result, the monomolecular and bimolecular cracking reactions [82-87] (Figure 12) occurred under the experimental conditions and the consecutive reaction of light olefins proceeded to form aromatics. Accordingly, the suppression of aromatic formation is indispensable to an increase in olefin yields, as for the ATO reaction discussed below.

Propylene and butylene were the primary products from *n*-hexane cracking, followed by production of aromatics and coke through a series of reactions, indicating that diffusion of the light olefins produced within the zeolite affected product yields and catalyst lifetime. Therefore, the effect of zeolite crystal size on product selectivity and catalytic stability in *n*-hexane cracking was investigated. Changes in *n*-hexane conversion and product yields over ZSM-5 zeolites (Si/Al = 150) with different crystal sizes are shown in Fig. 13 and Table 1. Although these ZSM-5 zeolites with different crystal sizes exhibited similar *n*-hexane conversion at the initial reaction time, the conversion gradually decreased with time in the macro-sized MFI-type zeolite, decreasing to 85% after 16 h. In contrast, the nano-sized MFI-type zeolite maintained a high conversion of 93% after 16 h, a minimal change from the start of the reaction. Additionally, the changes in light olefin and BTX yields with time in the nano-sized zeolite were different from the macro-sized zeolite. As shown in Fig. 13 and Table 1, the total yield of light olefins in the nano-sized zeolite (36.1%) was much greater than that in the macro-sized zeolite (23.1%) at the initial reaction time, and remained the same for 18 h, whereas BTX and olefin yields in the macro-sized zeolite monotonically changed with time.

The amounts of coke formed on the nano- and macro-sized zeolites during cracking were 2.2 wt% and 7.3 wt%, respectively. Although the nano-sized zeolite possessed a much larger external surface area than the macro-sized zeolite, the amount of coke formed on the nano-sized zeolite was approximately three-fold less than that formed on the macro-sized zeolite. Thermal cracking of *n*-hexane was negligibly small at the reaction temperature, hence, the coke on the

zeolites was derived from carbonaceous solid produced from catalytic cracking rather than thermal cracking. Since diffusion resistance of the light olefin products increased with crystal size, excessive reaction of light olefins must have occurred in the macro-sized zeolite, leading to an increase in BTX formation and coke deposition. In contrast, because diffusion resistance of the light olefin products was low within the nano-sized zeolite, excessive reaction was suppressed, leading to an increase in the yield of light olefins as well as suppression of coke formation. As a result, the nano-sized zeolite exhibited stable activity with high yield of light olefins when compared to the macro-sized zeolite.

4.4 Acetone-to-Olefins (ATO) Reaction over Nano-Sized Zeolite

In an ATO reaction, isobutylene is produced primarily from aldol condensation products of acetone (ATO reaction) over solid acid catalysts [65-71] in accordance with two reaction pathways in which a dimer and a trimer of acetone are decomposed to produce isobutylene [26, 39], as shown in Fig. 14. The relation between the pore sizes of zeolites and these intermediates are summarized in Table 2. Since trimers of acetone (pholone and iso-pholone) can be formed in beta zeolite (BEA zeolite, 12-membered rings), isobutylene and aromatics are observed as major products [39, 88], where cyclic compounds of iso-pholone can be formed within the micropore of beta zeolite and converted into aromatics. When using ZSM-5 (MFI zeolite, 10-membered rings), isobutylene is formed within the crystal pore by decomposition of diacetone alcohol (dimer), not

by decomposition of an acetone trimer (pholone and iso-pholone), due to spatial limitations of the MFI zeolite (10-membered rings) [25, 26]. In contrast, when using SAPO-34 (CHA zeolite, 8-membered rings), the aldol condensation of acetone proceeds mostly on the acid site located on the external surface, where the acetone dimer and trimers are formed, followed by decomposition to produce isobutylene, because the pore size of SAPO-34 is smaller than the molecular size of acetone [89]. The isobutylene produced reacts with itself to produce C_8 hydrocarbons followed by cyclization/cracking to form C_8 aromatics (xylene) and propylene [76]. Accordingly, the light olefins are intermediate chemicals in a series of reactions with aromatics and coke as the terminal products.

The ATO reaction was conducted over ZSM-5 zeolites with different crystal sizes using a fixed-bed reactor at a reaction temperature of 723K under an N_2 flow at atmospheric pressure. The *W/F* (W: amount of catalyst /g; F: feed rate /g h^{-1}) value was 0.5 h. The feed rate of acetone and the catalyst weight were 2.44×10^{-2} mol/h and 0.71 g, respectively. Composition of the exit gas was measured by on-line gas chromatography (GC-8A, Shimadzu Co. Ltd.) using a Porapak-Q column for an FID detector. The amount of coke deposited on the catalyst after reaction was measured by thermogravimetry (TG; TGA-50, Shimadzu Co. Ltd.).

Changes in acetone conversion with time on stream over the macro- and nano-sized zeolites can be seen in Fig. 15. Although the zeolites used as catalysts possessed nearly the same crystallinity and acidity, changes in acetone conversion with time were very different for the two zeolites. While acetone conversion in the macro-sized zeolite decreased to approximately 40%

after 6.5 h, at that time the conversion for the nano-sized zeolites was greater than 70% and decreased to 40% after 16 h. The amount of coke formed on the catalyst as measured by TG was 8.5 wt% and 8.2 wt% on the macro- and nano-sized zeolites, respectively. Although the nano-zeolite possessed a large external surface area compared to the macro-zeolite, the amount of coke formed on the nano-zeolite after reaction for 30 h was comparable to that of the macro-zeolite for 6.5 h. Thus, the decrease in crystal size of the zeolites suppressed coke formation, because the light olefins produced readily diffuse out of the intracrystalline pores of the nano-zeolite due to low diffusion resistance, suppressing of excessive reaction and coke formation. Thus, the decrease in crystal size of the zeolite is effective for stabilizing the catalytic activity in the ATO reaction.

Although the decrease in crystal size of the zeolite improved catalytic activity and stability, the catalyst lifetime was not long enough. Because deactivation of the zeolite catalyst during the ATO reaction was caused by coking, suppressing excessive reaction of the lighter olefins is essential for improving catalyst life, which can be achieved by modification of the acid sites through ion-exchange [39] or CCS [26] methods. Here, SiO_2 formation in the CCS method using phenyl-silane (P-silane) was applied to modify acidity of the nano-sized zeolite. The NH_3-TPD profiles of the nano-zeolite before and after CCS treatment can be seen in Fig. 8. Because the molecular size of PS is slightly smaller than the pore diameter of the MFI-type zeolite, acid sites on the external surface and on the internal surface are weakened. Accordingly, the amount of NH_3 desorbed from the strong acid sites decreased after CCS treatment due to formation of SiO_2 units

on the acid sites. In addition, since the intracrystalline pore size decreases slightly due to SiO_2 unit formation on the acid sites, the spatial limitation effect is expected to improve suppression of aromatics formation within the pore.

Changes in acetone conversion with time and product yield are shown in Fig. 15 and Table 3, respectively. Compared with the nano-zeolite before CCS treatment, the CCS-treated nano-zeolite exhibited stable activity with high acetone conversion of approximately 80% in 90 h. Moreover, CCS treatment of the nano-zeolite improved light olefin yields and suppressed aromatics formation as compared with macro- and nano-zeolites before CCS treatment. The improvement in catalytic stability and product selectivity was attributed to suppression of excessive reaction of the light olefins. As mentioned earlier, because the pores of ZSM-5 zeolite are too narrow to allow formation of acetone trimer, isobutylene is produced mainly by decomposition of the acetone dimer. CCS treatment using P-silane weaken acid sites with the narrow pore spaces of ZSM-5 zeolite, as compared with ZSM-5 before CCS treatment, leading to termination of the series of reactions that produce isobutylene form acetone dimers, shown in Fig. 13. Moreover, the decrease in crystal size of the zeolite enabled the isobutylene produced to diffuse out of the zeolite pore. As a result, the nano-zeolite treated with P-silane was an effective catalyst for the ATO reaction to produce light olefins at high yield with long catalyst life.

5. Conclusions

This review introduces size-controlled synthesis of nano-zeolites and their application as heterogeneous catalysts, which revealed that a reduction in crystal size led to improved catalytic properties for *n*-hexane cracking and the acetone-to-olefin reaction.

The effects of ionicity of the hydrophilic group of surfactant molecules and of the concentration of the Si source on the crystallinity and morphology of silicalite-1 were investigated. Results indicated that ionicity of the hydrophilic groups of the surfactant molecules played an important role in the formation and crystallization of nano-silicalite-1. When using non-ionic surfactant, mono-dispersed silicalite-1 nanocrystals approximately 60 nm in diameter were prepared successfully in a water-surfactant-organic solvent (emulsion method). The hydrophilic poly-oxyethylene chains in the surfactant can be adsorbed on the zeolite surface. The surfaces of the zeolite precursor and crystals were stabilized by the adsorbed surfactants, which enhanced the nucleation rate of zeolite followed by formation of mono-dispersed and size-controlled zeolites. To investigate the effect of crystal size of ZSM-5 zeolite on catalytic stability and light olefin yield, nano- and macro-zeolites with crystal sizes of approximately 150-200 nm and 1.5 μm, respectively, were prepared, and these catalysts were applied to *n*-hexane cracking and the acetone-to-olefins reactions.

In the catalytic cracking of *n*-hexane, the nano-sized zeolite exhibited high *n*-hexane conversion with stable activity for 18 h compared to the macro-sized zeolite. The high activity of the nano-zeolite is considered to be due to rapid diffusion of the light olefins out of the intracrystalline

pores of the nano-zeolite due to low diffusion resistance. Accordingly, the nano-sized zeolite exhibited high and stable activity with low coke formation compared with the macro-sized zeolite.

In the acetone-to-olefin reaction (ATO reaction), the nano-zeolite exhibited high activity over a long life when compared to the macro-zeolite. However, undesirable reactions that formed aromatics from the light olefins occurred. To suppress aromatics formation, deactivation of the acid sites of the zeolite was examined *via* the catalytic cracking of silane (CCS) using phenyl-silane (P-silane). The CCS method was effective in decreasing the acidity of the nano-zeolites. After CCS treatment using P-silane, the nano-zeolite maintained a high catalytic activity for more than 90 h, and exhibited high olefin yield (greater than 56 C-mol%).

Acknowledgements

This work was partly supported by the Research Grant Program from the New Energy and Industrial Technology Development Organization (NEDO) of Japan.

References

1. Ogura M, Shinomiya S, Tateno J, Nara Y, Nomura M, Kikuchi E, Matsukata M (2001) Appl Catal A Gen 219:33
2. Groen JC, Peffer LAA, Moulijn JA, Perez-Ramirez J (2004) Micropore Mesopor Mat 69:29
3. Groen JC, Jansen JC, Moulijn JA, Perez-Ramirez J (2004) J Phys Chem B 108:13062
4. Tsapatsis M, Lovallo M, Davis ME (1996) Micropor Mat 5:381

5. Ravishankar R, Kirschhock C, Schoeman BJ, Vanoppen P, Grobet PJ, Storck S, Maier WF, Martens JA, DeSchryver FC, Jacobs PA (1998) J Phys Chem B 102:2633

6. Mintova S, Olson NH, Valtchev V, Bein T (1999) Science 283:958

7. Grieken RV, Sotelo JL, Menendez JM, Melero JA (2000) Micropor Mesopor Mat 39:135

8. Mintva S, Valtchev V (2002) Micropor Mesopor Mat 55:171

9. Hincapie BO, Garces LJ, Zhang Q, Sacco A, Suib SL (2004) Micropor Mesopor Mat, 67:1387

10. Song W, Justice RE, Jones CA, Grassian VH, Larsen SC (2004) Langmuir 20:4696

11. Song W, Justice RE, Jones CA, Grassian VH, Larsen SC (2004) Langmuir 20:8301

12. Song W, Grassian VH, Larsen SC (2005) Chem Comm 23:2951

13. Larlus O, Mintova S, Bein T (2006) Micropor Mesopor Mat 96:405

14. Mintova S, Valtchev V, Onfroy T, Marichal C, Knozinger H, Bein T (2006) Micropor Mesopor Mat 90:237

15. Morales-Pacheco P, Alvarez F, Del Angel P, Bucio L, Dominguez JM (2007) J Phys Chem C 111:2368

16. Kumar S, Davis TM, Ramanan H, Penn RL, Tsapatsis M (2007) J Phys Chem B 111:3393

17. Tosheva L, Valtchev VP (2005) Chem. Mater 7:2494

18. Larsen SC (2007) J Phys Chem C 111:18464

19. Tago T, Nishi M, Kouno Y, Masuda T (2004) Chem Lett 33:1040

20. Tago T, Iwakai K, Nishi M, Masuda T (2006) Stud Surf Sci Catal 159:185

21. TagoT, Iwakai K, Nishi M, Masuda T (2009) J Nanosci Nanotechnol 9:612

22. Tago T, Aoki D, Iwakai K, Masuda T (2009) Top Catal 52:865

23. Iwakai K, Tago T, Konno H, Nakasaka Y, Masuda T (2011) Micropor Mesopor Mat 141:167

24. Masuda T, Fukumoto N, Kitamura M, Mukai SR, Hashimoto K, Tanaka T, Funabiki T (2001) Micropor Mesopor Mat 48:239

25. Tago T, Sakamoto M, Iwakai K, Nishihara H, Mukai SR, Tanaka T, Masuda T (2009) J Chem Eng Jpn 42:162

26 Tago T, Konno H, Sakamoto M, Nakasaka Y, Masuda T (2011) Appl Catal A Gen 403:183

27. Naik SP, Chen JC, Chiang AST (2002) Micropor Mesopor Mat 54:293

28. Lee S, Carr CS, Shantz DF (2005) Langmuir 21:12031

29. Kuechl DE, Benin AI, Knight LM, Abrevaya H, Wilson ST, Sinkler W, Mezza TM, Willis RR (2010) Micropor Mesopor Mat 127:104

30. Burkett SL, Davis ME (1994) J Phys Chem 98:4647

31. Burkett SL, Davis ME (1995) Chem Matter 7:920

32. DeMoor PPEA, Beelen TPM, Komanschek BU, Beck LW, Wagner P, Davis ME, Santen RA (1999) Chem Eur J 5:2083

33. DeMoor PPEA, Beelen TPM, Van Santen RA (1999) J Phys Chem C 103:1639

34. Mitsui T, Machida Y (1969) J Soc Cosmetic Chemists 20:199

35. Fukuoka T, Morita T, Konishi M, Imura T, Sakai H, Kitamoto D (2007) App Microbiol Biotechnol 76:801

36. Niwa M, Murakami Y (1989) J Phys Chem Sol 50:487

37. Niwa M, Yamazaki K, Murakami Y (1991) Ind Eng Chem Res 30:38

38. Katada N, Niwa M (1996) Chem Vap Dep 2:125

39. Tago T, Konno H, Ikeda S, Yamazaki S, Ninomiya W, Nakasaka Y, Masuda T (2011) Catal Today 164:158

40. Masuda T, Asanuma T, Shouji M, Mukai SR, Kawase M, Hashimoto K (2003) Chem Eng Sci 58:649

41. Tago T, Iwakai K, Morita K, Tanaka K, Masuda T (2005) Catal Today 105:662

42. Botella P, Corma A, Iborra S, Montón R, Rodríguez I, Costa V (2007) J Catal 250:161

43. Serrano DP, Aguado J, Escola JM, Rodriguez JM (2005) J Anal Appl Pyrol 74:353

44. Choi M, Na K, Kim J, Sakamoto Y. Terasaki O, Ryoo R (2009) Nature 461:246

45. Na K, Jo C, Kim J, Cho K, Jung J, Seo Y, Messinger RJ, Chmelka BF, Ryoo R (2011) Science 333:328

46. Rhodes KH, Davis SA, Caruso F, Zhang BJ, Mann S (2000) Chem Mater 12:2832

47. Groen JC, Peffer LAA, Perez-Ramirez J (2003) Micropor Mesopor Mat 60:1

48. Srivastava R, Choi M, Ryoo R (2006) Cem Commun 43:4489

49. Shetti VN, Kim J, Srivastava R, Choi M, Ryoo R. (2008) J Catal 254:296

50. Serrano DP, Aguado J, Escola JM, Rodriguez JM, Peral A (2006) Chem Mat 18:2462

51. Perez-Ramirez J, Christensen CH, Egeblad K, Christensen CH, Groen JC (2008) Chem Soc Rev 37:2530

52. Serrano DP, Aguado J, Escola JM, Rodriguez JM, Peral A (2008) J Mater Chem 18:4210

53. Serrano DP, Aguado J, Escola J M, Rodriguez JM, Peral A (2010) J Catal 276:152

54. Serrano DP, Sanz R, Pizarro P, Moreno I (2009) Chem Commun 11:1407

55. Yosimura Y, Kijima N, Hayakawa T, Murata K, Suzuki K, Mizukami F, Matano K, Konishi T, Oikawa T, Saito M, Shiojima T, Shiozawa K, Wakui K, Sawada G, Sato K, Matsuo S, Yamaoka N (2000) Catal Surv Jpn 4:157

56. Magnoux P, Cartraud P, Mignard S, Guisnet M (1987) J Catal 106:242

57. Corma A, Gonzàlez-Alfaro V, Orchillès AV **(1995)** Appl Catal A Gen 129:203

58. Katada N, Kageyama Y, Takahara K, Kanai K, Beguma HA, Niwa M (2004) Catal A Chem 211:119

59. Stocker M (1999) Micropor Mesopor Mater 29:3

60. Keil FJ (1999) Micropor Mesopor Mater 29:49

61. Dahl IM, Wendelbo R, Andersen A, Akporiaye D, Mostad H, Fuglerud T(1999) Micropor Mesopor Mater 29:159

62. Oikawa H, Shibata Y, Inazu K, Iwase Y, Murai K, Hyodo S, Kobayashi G, Baba T (2006) Appl Catal A Gen 312:181

63. Mentzel UV, Holm MS (2011) Appl Catal A Gen 396:59

64. Gayubo, AG, Valle B, Aguayo AT, Olazar M, Bilbao J (2010) Ind Eng Chem Res 49:123

65. Novakova J, Kubelkova L, Dolejsek Z (1987) J Molec Catal 39:195

66. Kubelkova L, Cejka J, Novakova J (1991) Zeolite 11:48

67. Kubelkova L, Novakova J (1991) Zeolite 11:822

68. Biaglow AI, Sepa J, Gorte RJ, White D (1995) J Catal 151:373

69. Panov, AG, Fripiat JT (1998) J Catal 178:188

70. Panov A, Fripiat JJ (1998) Langmuir 14:3788

71. Song WG, Nicholas JB, Haw JF (2001) J Phys Chem B 105:4317

72. Corma A, Martinez-Triguero J (1997) J Catal 165:102

73. Inagaki S, Takechi K, Kubota Y (2010) Chem Commun 46:2662

74. Kotrel S, Rosynek MP, Lunsford JH (2000) J Catal 191:55

75. Babitz SM, Williams BA, Miller JT, Snurr RQ, Haag WO, Kung HH (1999) Appl Catal A Gen 179:71

76. Wielers AFH, Waarkamp M, Post MFM (1991) J Catal 127:51

77. Mochizuki H, Yokoi T, Imai H, Watanabe R, Namba S, Kondo JN, Tatsumi T (2011) Micropor Mesopor Mater 145:165

78. Kimura T, Gao J, Sakashita K, Li XH, Asaoka S (2012) J Jpn Petrol Inst 55:40

79. Konno H, Okamura T, Nakasaka Y, Tago T, Masuda T, J Jpn Petrol Inst in press

80. Babitz SM, Williams BA, Miller JT, Snurr RQ, Haag WO, Kung HH (1999) Appl Catal A Gen 179:71

81. Williams BA, Babitz SM, Miller JT, Snurr RQ, Kung HH, Appl Catal A Gen (1999) 177:161

82. Williams BA, Ji W, Miller JT, Snurr RQ, Kung HH (2000) Appl Catal A Gen 203:179

83. Haag W O, Dessau RM (1984) Proc 8th Int Congr Catal, Berlin, 2:305

84. Jolly S, Saussey J, Bettahar MM, Lavalley JC, Benazzi E (1997) Appl Catal A Gen 156:71

85. Corma AV, Orchillès AV (2000) Micropor Mesopor Mater 35–36:21

86. Komatsu T, Ishihara H, Fukui Y, Yashima T (2001) Appl Catal A Gen 214:103

87. Kotrel S, Knozinger H, Gates BC (2006) *Micropor Mesopor Mater* 35-36:11

88. Cruz-Cabeza AJ, Esquivel D, Jimenez-Sanchidrian C, Romero-Salguero FJ (2012) Materials 5:121

89. Hirota Y, Nakano Y, Watanabe K, Uchida Y, Miyamoto M, Egashira Y, Nishiyama N (2012) Catal Lett 142:464

Figure Captions

Fig. 1 Zeolite structure, pore size and molecular diameter of hydrocarbons

Fig. 2 FE-SEM micrographs of samples prepared in the water/surfactant/organic solvent showing effects of ionicity of the surfactant on morphology of the silicalite-1 (MFI zeolite)

Fig. 3 Relation between composition of the water-surfactant-organic solvent and crystal size and morphology of silicalite-1

Fig. 4 Schematic diagram showing zeolite nucleation, crystal growth, and possible relation between the surfactant and zeolite surface

Fig. 5 Relation between HLB values of surfactant and amount of adsorbed N_2

Fig. 6 Experimental procedure and relation between molecular sizes of the silane compounds and the regioselective deactivation of acid sites by the CCS method

Fig. 7 Changes in acidity of beta zeolite (BEA zeolite) after (a) alkali metal ion-exchange and (b) CCS (P-silane) treatments

Fig. 8 Changes in acidity of ZSM-5 zeolite (MFI zeolite) after CCS treatments using phenyl-silane compounds of different molecular sizes

Fig. 9 FE-SEM micrographs of macro- and nano-ZSM-5 zeolites (Si/Al=80)

Fig. 10 NH_3-TPD profiles of nano- and macro-ZSM-5 zeolites with different Si/Al ratios

Fig. 11 Relation between product yield and *n*-hexane conversion for reaction over nano-ZSM-5 zeolites with different Si/Al ratios

Fig. 12 Schematic diagram of the alkane cracking reaction over acid catalysts based on mono- and bi-molecular mechanisms

Fig. 13 Changes in *n*-hexane conversion and product yields with time over (a) macro- and (b) nano-zeolites (Si/Al = 50)

Fig. 14 Reaction pathways for olefins synthesis from acetone over solid-acid catalyst

Fig. 15 Acetone conversions over macro- and nano-ZSM-5 zeolites before and after CCS treatment (Si/Al = 80)

Table 1 *n*-Hexane conversion and product yields from *n*-hexane cracking over macro- and nano-zeolites

Table2 Possible relation between zeolite pore size and intermediates for ATO reactions

Table 3 Acetone conversion and product yields from the ATO reaction over macro- and nano-zeolites before and after CCS treatment using P-silane

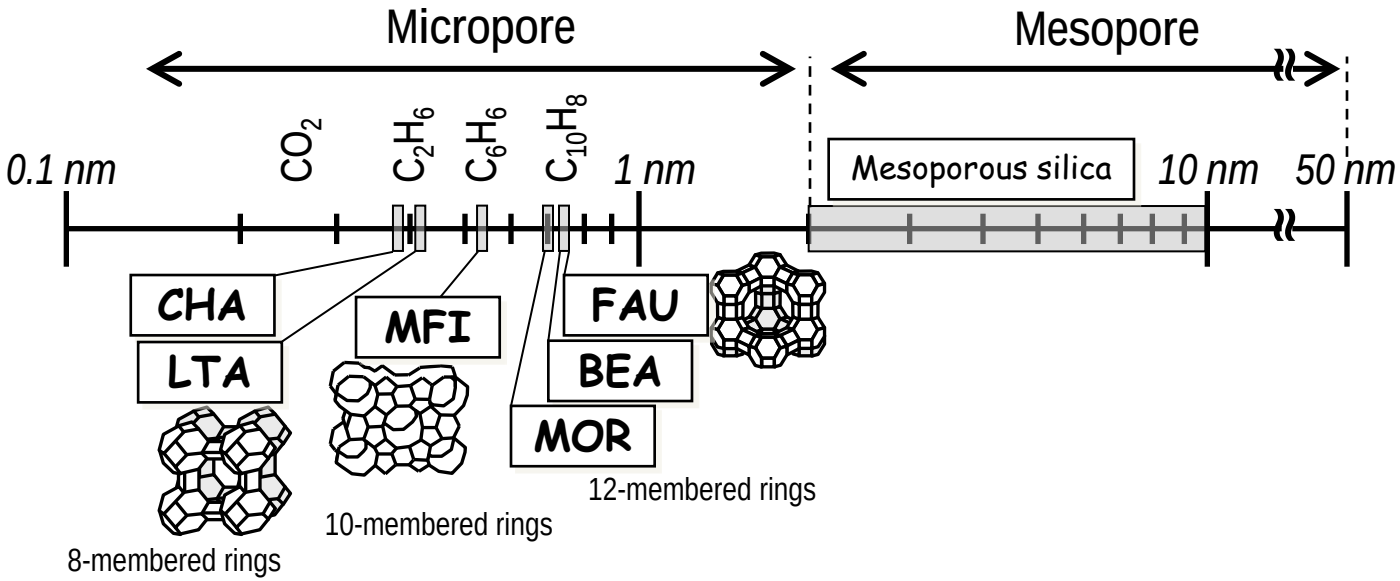

Fig. 1 Zeolite structure, pore size and molecular diameter of hydrocarbons

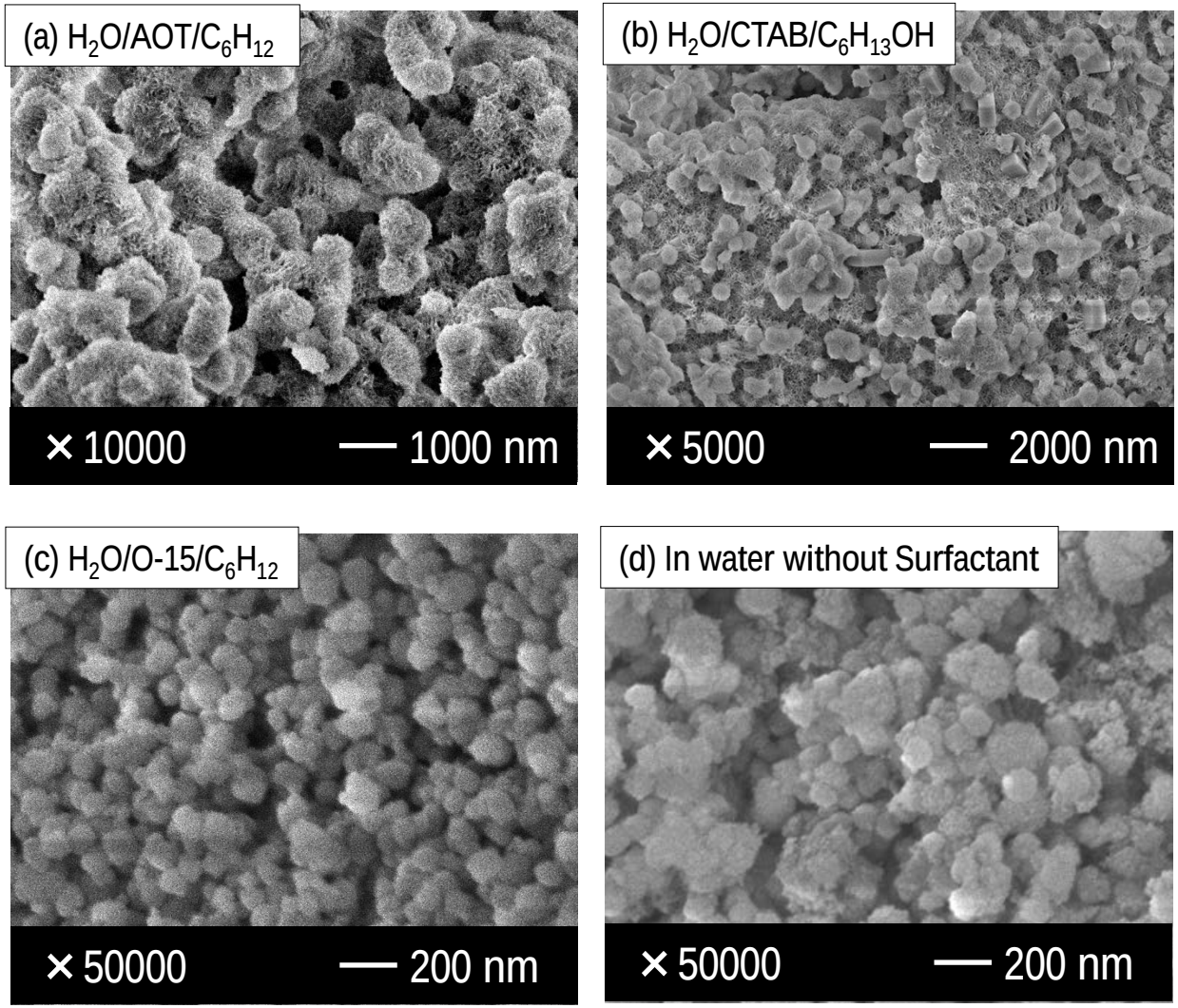

Fig. 2 FE-SEM micrographs of samples prepared in the water/surfactant/organic solvent showing effects of ionicity of the surfactant on morphology of the silicalite-1 (MFI zeolite)

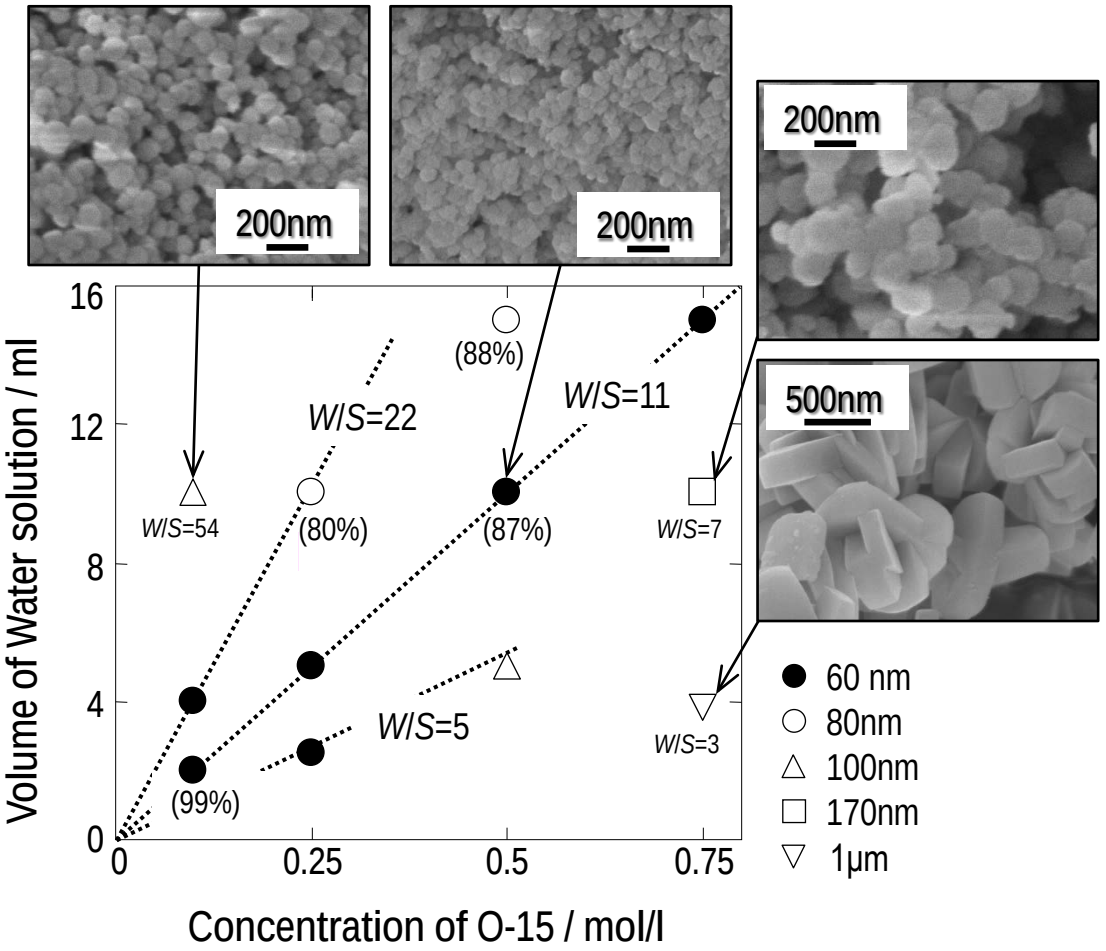

Fig. 3 Relation between composition of the water-surfactant-organic solvent and crystal size and morphology of silicalite-1

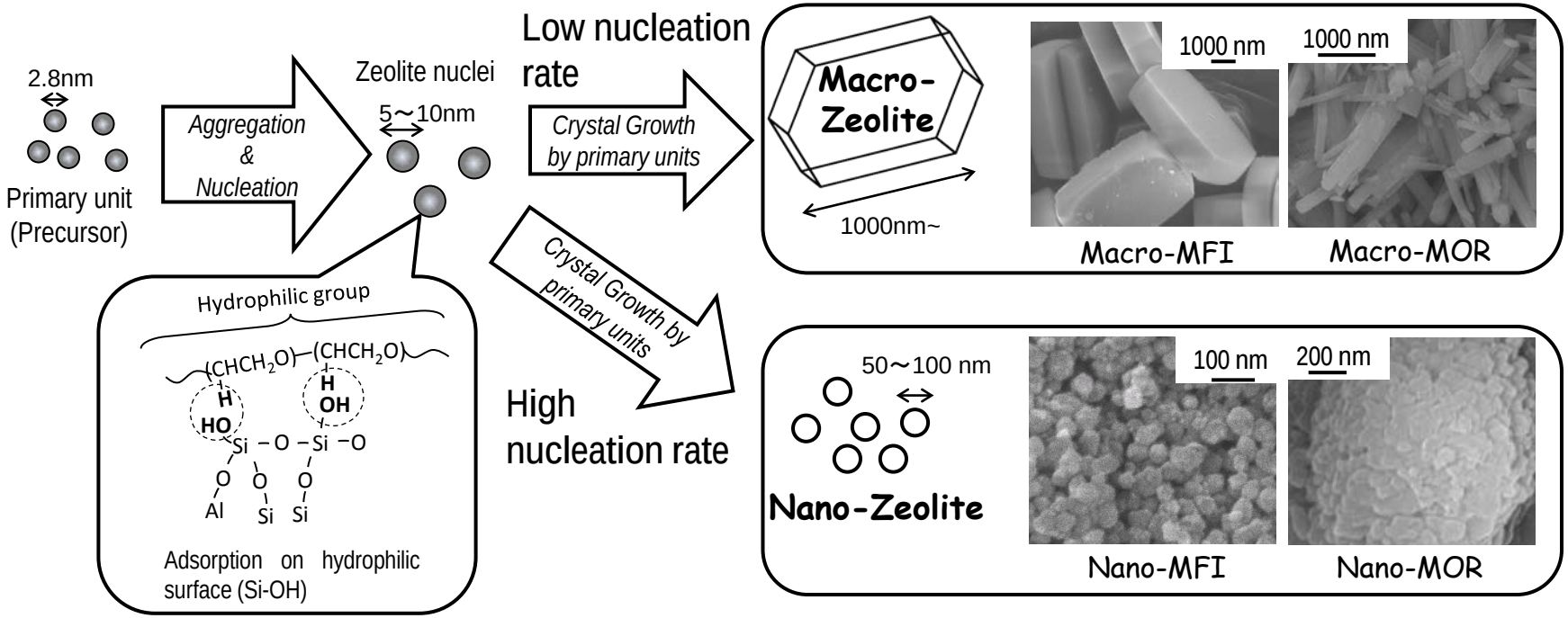

Fig. 4 Schematic diagram showing zeolite nucleation, crystal growth, and possible relation between the surfactant and zeolite surface

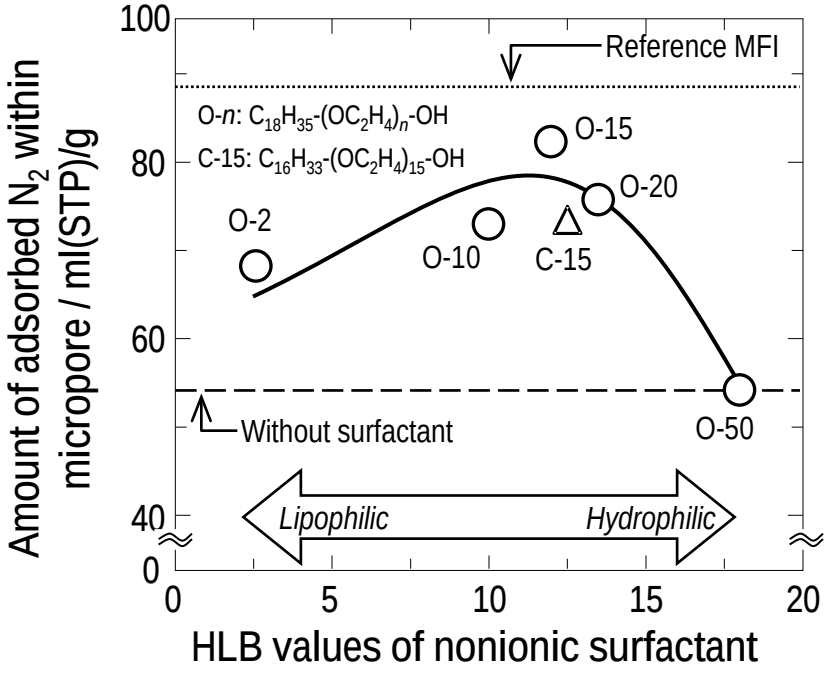

Fig. 5 Relation between HLB values of surfactant and amount of adsorbed N_2

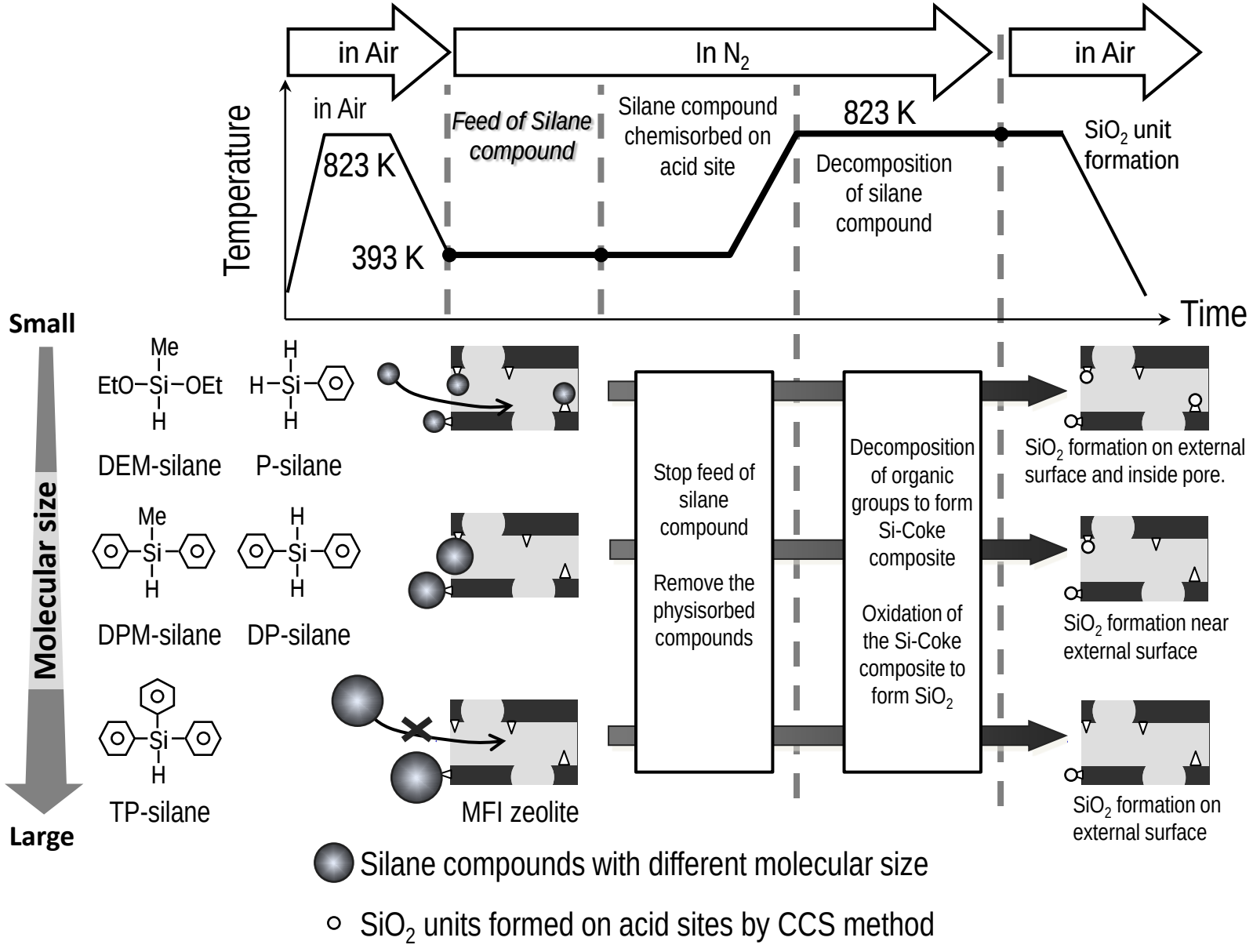

Fig. 6 Experimental procedure and relation between molecular sizes of the silane compounds and the regioselective deactivation of acid sites by the CCS method

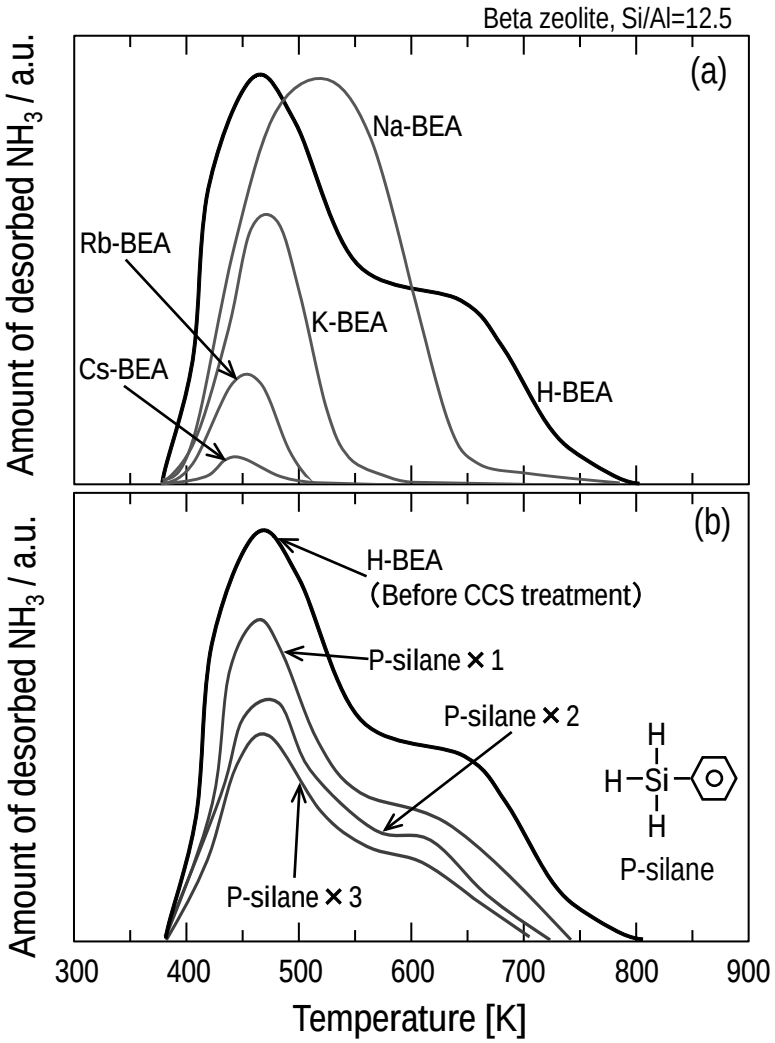

Fig. 7 Changes in acidity of beta zeolite (BEA zeolite) after (a) alkali metal ion-exchange and (b) CCS (P-silane) treatments

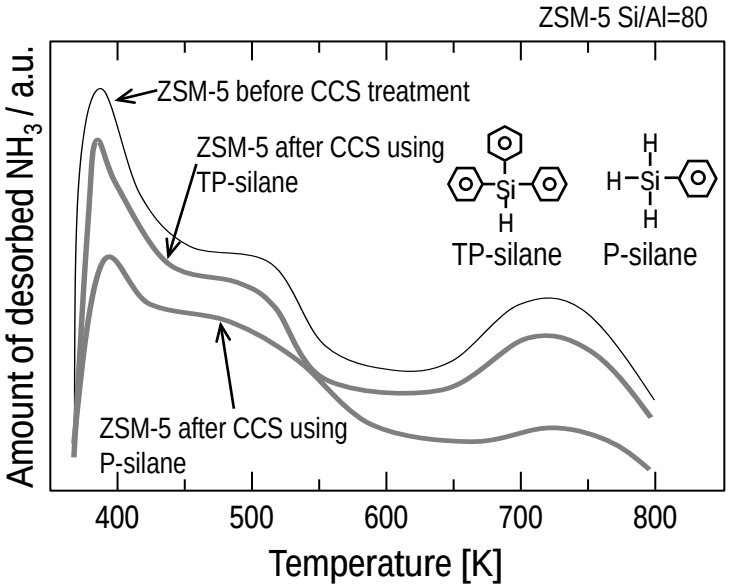

Fig. 8 Changes in acidity of ZSM-5 zeolite (MFI zeolite) after CCS treatments using phenyl-silane compounds of different molecular sizes

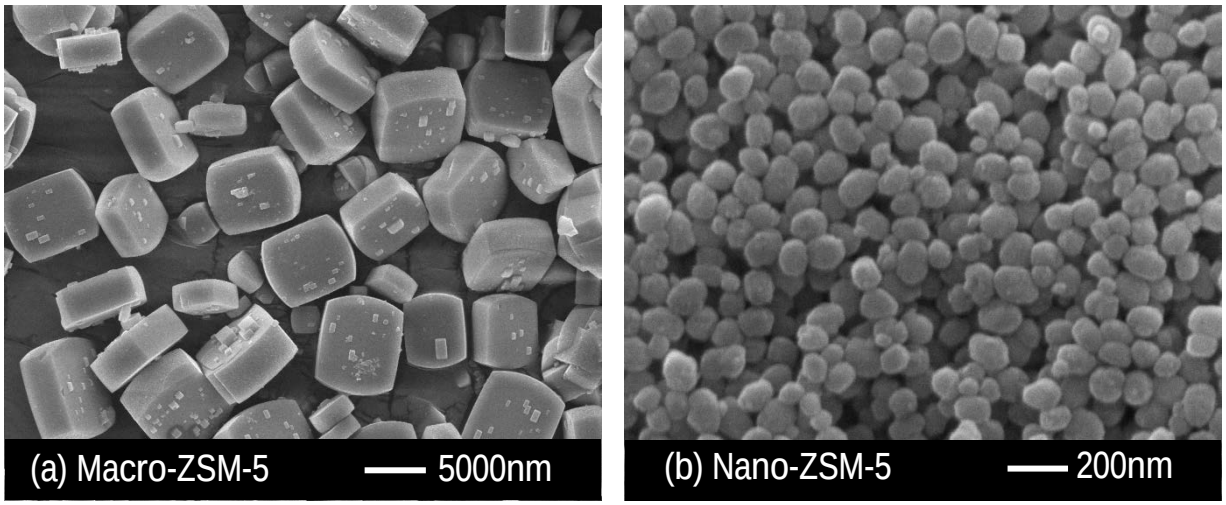

Fig. 9 FE-SEM micrographs of macro- and nano-ZSM-5 zeolites (Si/Al=80)

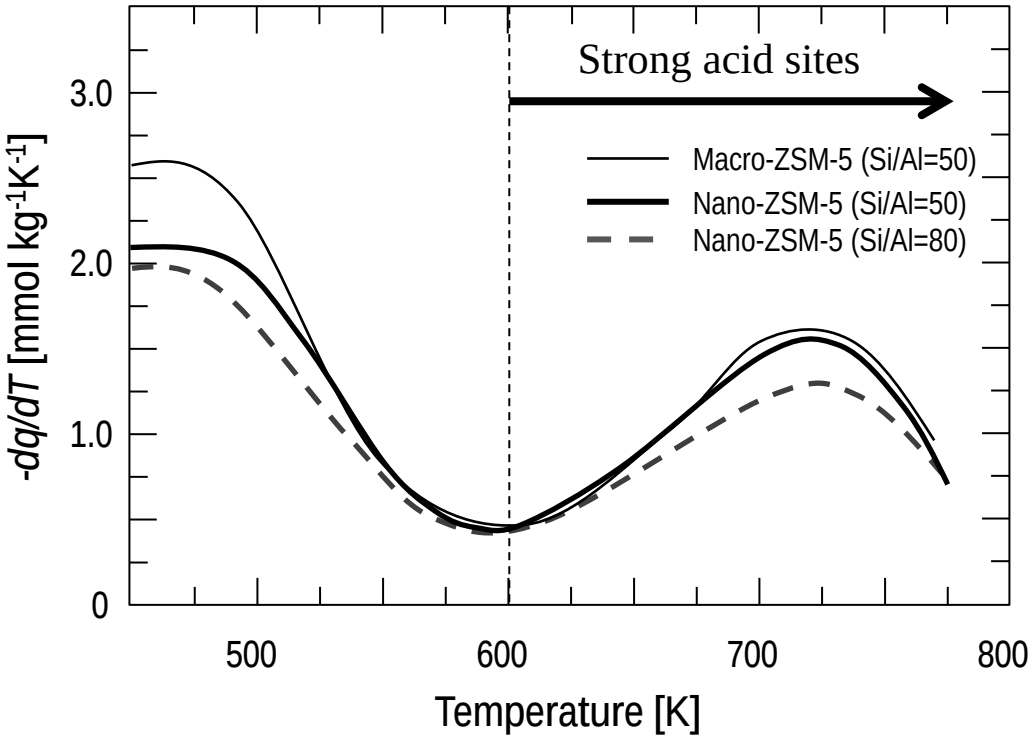

Fig. 10 NH_3-TPD profiles of nano- and macro-ZSM-5 zeolites with different Si/Al ratios

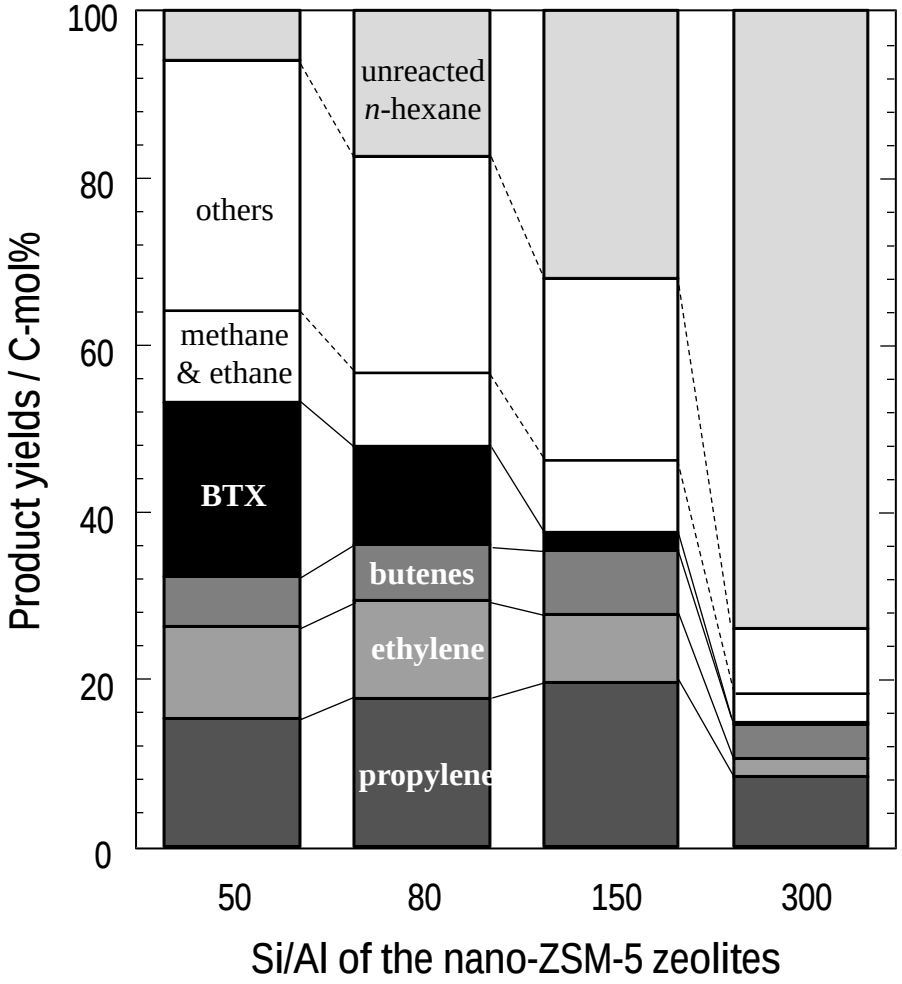

Fig. 11 Relation between product yield and *n*-hexane conversion for reaction over nano-ZSM-5 zeolites with different Si/Al ratios

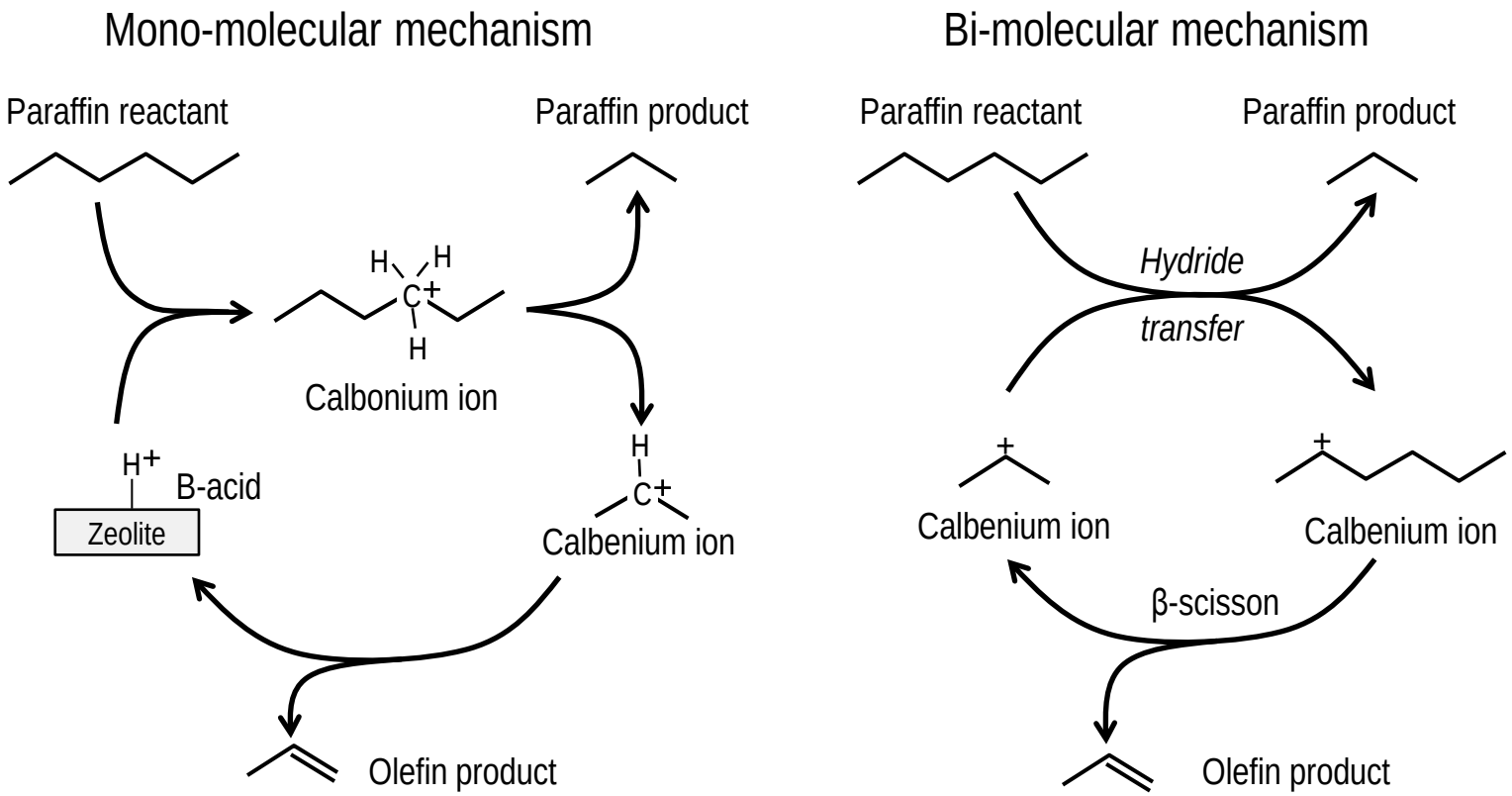

Fig. 12 Schematic diagram of the alkane cracking reaction over acid catalysts based on mono- and bi-molecular mechanisms

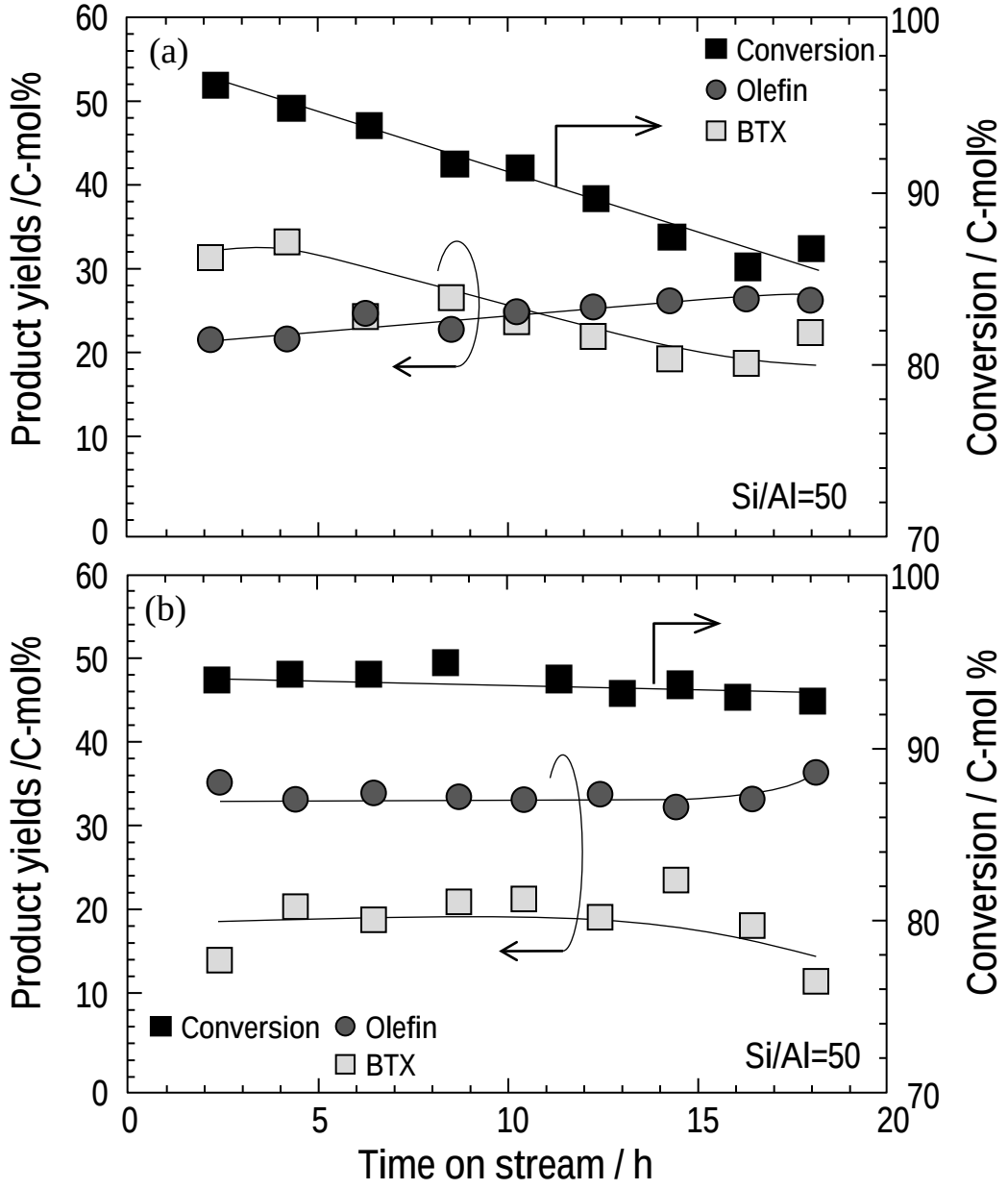

Fig. 13 Changes in *n*-hexane conversion and product yields with time over (a) macro- and (b) nano-zeolites (Si/Al = 50)

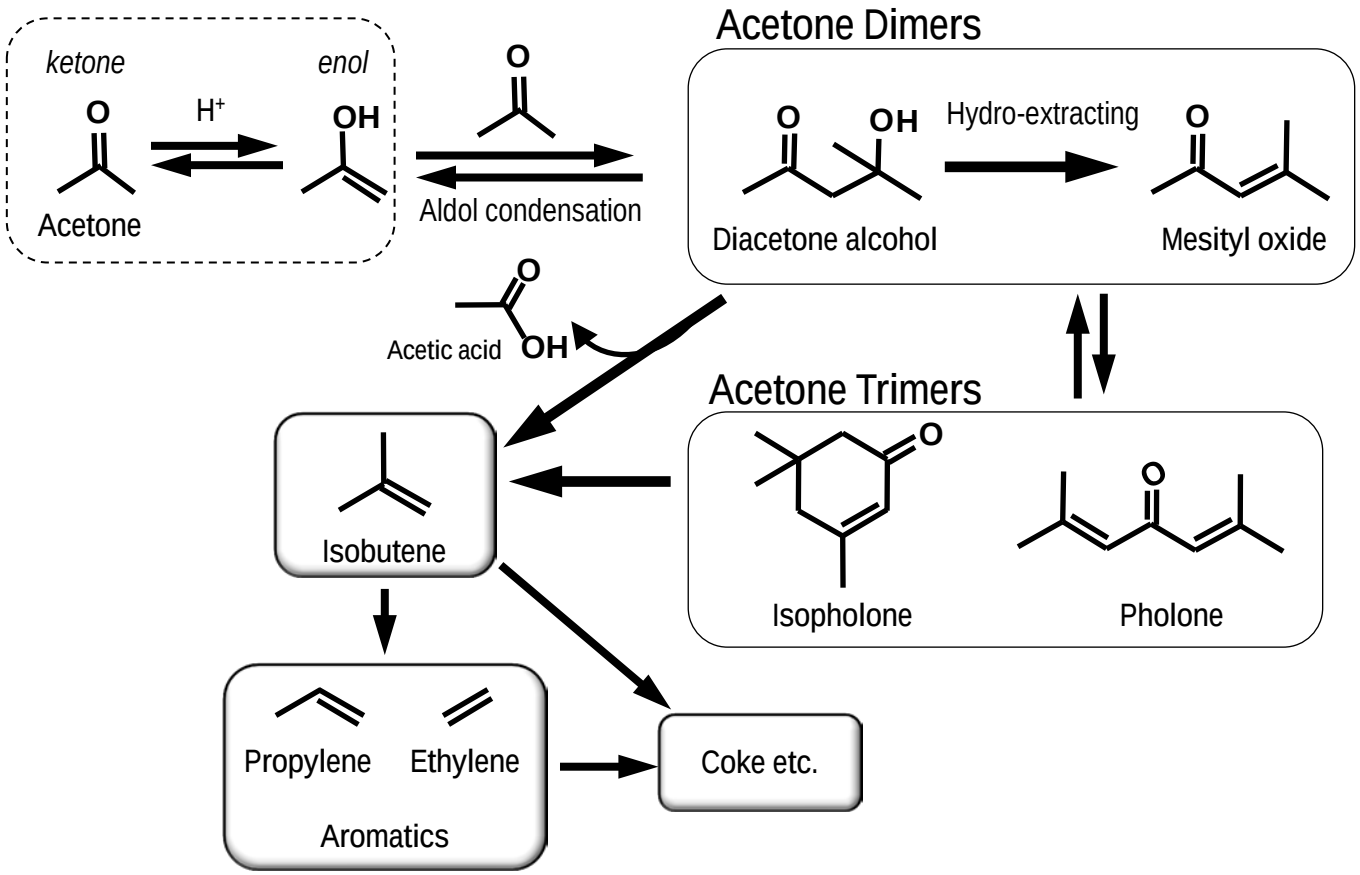

Fig. 14 Reaction pathways for olefins synthesis from acetone over solid-acid catalyst

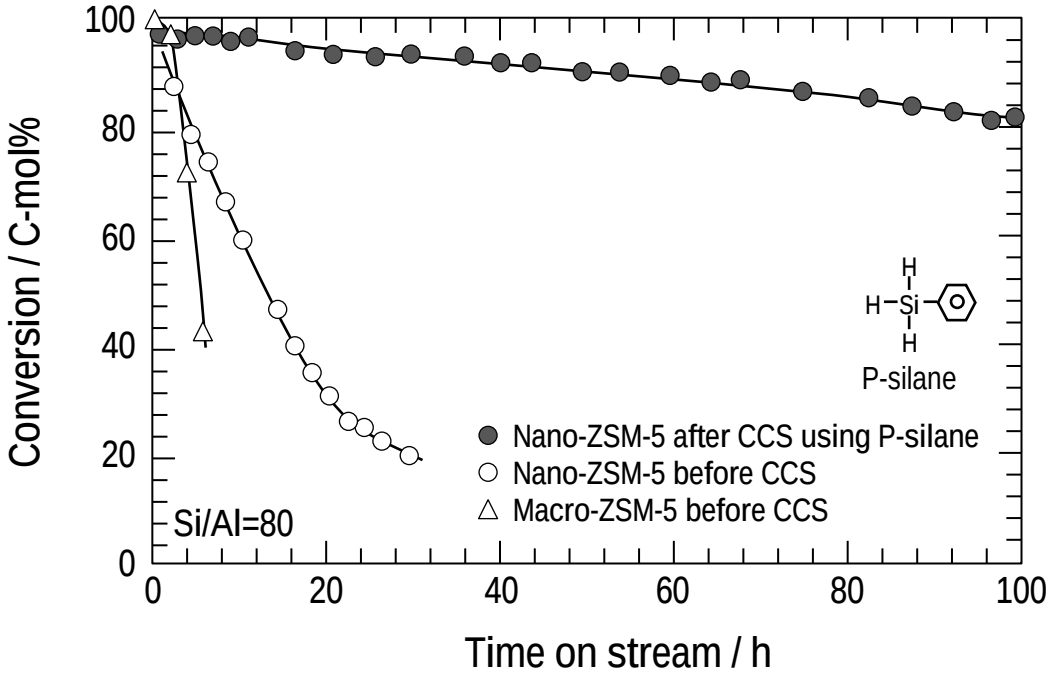

Fig. 15 Acetone conversions over macro- and nano-ZSM-5 zeolites before and after CCS treatment (Si/Al = 80)

Table 1 *n*-Hexane conversion and product yields from *n*-hexane cracking over macro- and nano-zeolites

Catalyst	Time [h]	**Conversion [C-mol%]**	Light olefins yield [C-mol%]				**BTX yield [C-mol%]**	Others yield [C-mol%]
			$C_2^=$	$C_3^=$	$C_4^=$	**Total olefins**		
Macro-ZSN-5	2.33	**96.2**	9.5	10.3	3.3	**23.1**	**32.5**	44.4
	18.0	**86.7**	9.5	13.6	4.5	**27.6**	**23.9**	48.5
Nano-ZSM-5	2.33	**93.7**	13.5	16.8	5.7	**36.0**	**15.4**	48.6
	18.0	**92.3**	13.7	17.3	6.0	**37.0**	**12.9**	50.1

Table2 Possible relation between zeolite pore size and intermediates for ATO reactions

Size of main channel	Typical framework type of zeolite	Intermediates for ATO reaction	
		Acid site locations	
		External surface (around pore mouth)	Pore surface inside crystal
8-membered ring	CHA LTA	Dimer Tirimer	X
10-membered ring	MFI	Dimer Tirimer	Dimer
12-membered ring	MOR, BEA FAU	Dimer Tirimer	Dimer Tirimer

Table 3 Acetone conversion and product yields from the ATO reaction over macro- and nano-zeolites before and after CCS treatment using P-silane

Catalyst	Time [h]	**Conversion [C-mol%]**	Light olefins yield [C-mol%]				**BTX yield [C-mol%]**	Others yield [C-mol%]
			$C_2^=$	$C_3^=$	$C_4^=$	**Total olefins**		
macroMFI	4.5	**71.7**	4.8	16.2	18.7	**39.7**	**15.3**	45.0
nanoMFI	6.5	**74.2**	3.1	16.7	19.5	**39.3**	**16.5**	44.2
CCS-nanoMFI	4.5	**97.0**	2.2	23.7	30.6	**56.5**	**9.8**	33.7
	99.2	**81.7**	0.3	4.3	51.7	**56.2**	**3.7**	40.1